

Equivariant Descriptor Fields: SE(3)-Equivariant Energy-Based Models for End-to-End Visual Robotic Manipulation Learning

Hyunwoo Ryu¹, Jeong-Hoon Lee², Hong-in Lee¹, and Jongeun Choi³

Abstract—End-to-end learning for visual robotic manipulation is known to suffer from sample inefficiency, requiring a large number of demonstrations. The spatial roto-translation equivariance, or the $SE(3)$ -equivariance can be exploited to improve the sample efficiency for learning robotic manipulation. In this paper, we present fully end-to-end SE(3)-equivariant models for visual robotic manipulation from a point cloud input. By utilizing the representation theory of the Lie group, we construct novel SE(3)-equivariant energy-based models that allow highly sample efficient end-to-end learning. We show that our models can learn from scratch without prior knowledge yet is highly sample efficient (~ 10 demonstrations are enough). Furthermore, we show that the trained models can generalize to tasks with (i) previously unseen target object poses, (ii) previously unseen target object instances of the category, and (iii) previously unseen visual distractors. We experiment with 6-DoF robotic manipulation tasks to validate our models' sample efficiency and generalizability. Codes are available at: <https://github.com/tomato1mule/edf>

I. INTRODUCTION

End-to-end learning for robotic manipulation often involves a lot of trials and errors due to explorations [1], [2], [3]. Learning from demonstration (LfD) [4], [5] methods are advantageous in that they do not involve any trials and errors since only expert demonstrations are used for training. However, expert demonstrations are often rare and expensive to collect. Therefore in visual robotic manipulation, common practices are to incorporate auxiliary pipelines such as pose estimation [6], [7], object segmentation [8], or pre-trained object representations [8], [9], [10] to improve the sample efficiency of LfD algorithms. However, sufficient data for training such pipelines are often unavailable in practice. Therefore, sample efficient end-to-end visual models are desirable.

Recently, group equivariant models have gained the spotlight for their sample efficiency in various domains such as protein folding and pose estimation tasks [11], [12], [13], [14]. Group equivariance is a property that if the input transforms by some group element, then the output should also transform accordingly.

For robotic manipulation, the roto-translation equivariance can be exploited for sample efficient learning. The roto-translation equivariance can be mathematically formalized

as the special Euclidean group $SE(n)$, where n denotes the dimension. Transporter Networks [15] achieve impressive sample efficiencies for end-to-end learning of planar tasks by exploiting the $SE(2)$ -equivariance, which is the planar roto-translation group. However, Transporter Networks cannot efficiently solve highly spatial tasks with non-planar roto-translation symmetries since they are not fully $SE(3)$ -equivariant.

Neural Descriptor Fields (NDFs) [8] have been proposed to incorporate full $SE(3)$ -equivariance in robotic manipulation. NDFs successfully learn to solve simple pick-and-place tasks with few demonstrations (5~10). In addition, NDFs can generalize to unseen poses and unseen instances (in the same object class) of the target objects. However, NDFs cannot be trained end-to-end. NDFs resort to self-supervised representations of the object's geometry, which require hard-to-collect voxel data of the target object categories for training. In addition, NDFs assume the object point cloud to be segmented from the background. These assumptions are highly non-trivial in practice. Therefore, fully $SE(3)$ -equivariant end-to-end models for sample efficient manipulation learning still need to be studied.

To this end, we propose the first fully end-to-end $SE(3)$ -equivariant models for visual robotic manipulation. Our method consists of two models, the picking model and the placing model. For the equivariance of the models, we propose *Equivariant Descriptor Fields* (EDFs), which are the representation-theoretic generalizations to NDFs [8]. We reformulate the energy optimization problem of [8] into a distribution learning problem by constructing representation-theoretic equivariant energy-based models. We also provide effective sampling strategies and training algorithms for our unnormalized energy-based models on the $SE(3)$ manifold. We show that our models are fully end-to-end yet are highly sample efficient (~ 10 demonstrations are enough). Moreover, We show that our trained models can generalize to previously unseen out-of-distribution (OoD) poses and unseen instances (in the same object class) of the target objects (See Fig. 1). We also show that our models can robustly solve tasks in the presence of unseen visual distractors.

The contributions of our paper are summarized as follows.

- We propose the first fully end-to-end $SE(3)$ -equivariant models for visual robotic manipulation.
- We introduce novel representation-theoretic energy functions that guarantee $SE(3)$ -equivariance.
- We generalize the invariant descriptors of NDFs into

¹H. Ryu and H. Lee are with the Department of Artificial Intelligence, Yonsei University, Seoul, Republic of Korea. {tomato1mule, theorist17}@yonsei.ac.kr

²J. Lee is with the School of Mechanical Engineering, Yonsei University, Seoul, Republic of Korea. ljh_0921@yonsei.ac.kr

³J. Choi is with the School of Mechanical Engineering and the Department of Artificial Intelligence, Yonsei University, Seoul, Republic of Korea. joungeunchoi@yonsei.ac.kr

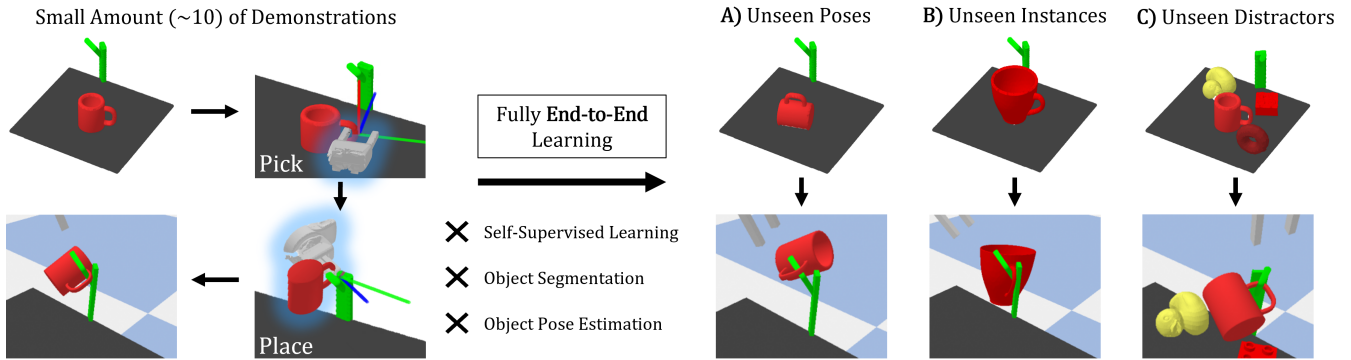


Fig. 1. Given a small amount (~ 10) of demonstrations, EDFs can learn to solve highly spatial pick-and-place tasks. The left side of the figure illustrates an example task demonstration where a mug (red) is picked and placed on a hanger (green). Note that EDFs work in a fully end-to-end manner without resorting to auxiliary algorithms such as pose estimation, segmentation, or self-supervised learning pipelines. We also show that the trained EDFs can generalize to A) unseen out-of-distribution poses of the target objects, B) unseen target object instances in the category, and C) the existence of unseen visual distractors.

the representation-theoretic equivariant descriptors.

- We reformulate the energy optimization problem of NDFs into a probability distribution learning problem.
- We provide sampling strategies and a training algorithm for our unnormalized energy-based models on the $SE(3)$ manifold.

II. BACKGROUNDS

A. Equivariant Robotic Manipulation Learning

Equivariant robotic manipulation learning is a branch of robot manipulation learning that exploits the symmetry of the tasks to improve sample efficiency in learning.

Consider the problem of finding the pose of the grasp T_{grasp} given an input X^1 . Let there be a symmetry group $g \in G$ such that it acts on T_{grasp} by a transformation T_g and acts on X by a transformation S_g . For sample efficiency, it would be desirable that the grasp pose be equivariant to the input. Then the problem can be formally defined as either learning an equivariant pose regressor f_θ

$$\begin{aligned} T_{grasp} &= f_\theta(X) \\ \text{s.t.} \quad T_g T_{grasp} &= f_\theta(S_g X) \end{aligned} \quad (1)$$

or learning an equivariant distribution (or policy) P_θ

$$\begin{aligned} T_{grasp} &\sim P_\theta(T_{grasp}|X) \\ \text{s.t.} \quad P_\theta(T_g T_{grasp}|S_g X) &= P_\theta(T_{grasp}|X) \end{aligned} \quad (2)$$

where θ denotes the learnable parameters.

1) *Transporter Networks*: Transporter Networks [15] are end-to-end models aimed at learning the target distribution of the grasp pose for pick-and-place tasks. By imposing the equivariance of the planar roto-translation group, $SE(2)$, the models are capable of learning simple tasks in a few-shot level ($1 \sim 10$ demonstrations). Moreover, the models are capable of learning complex sequential problems. However, Transporter Networks use group convolutional models [16] to obtain the equivariance. Group convolutional models require

¹Examples of commonly used inputs are color-depth images, point clouds, object positions.

the target symmetry group to be discretized and thus are prone to inaccuracy issues and the curse of dimensionality. It is prohibitively expensive to run group convolutional models for the $SE(3)$ group, which is a 6-dimensional manifold. Insufficient discretization often results in inaccuracy even for the $SE(2)$ group. As a result, Transporter networks are inefficient for highly spatial tasks with the $SE(3)$ symmetry.

2) *Neural Descriptor Fields*: Neural Descriptor Fields (NDFs) [8] have recently been proposed to fully incorporate the $SE(3)$ -equivariance in robotic manipulation. For a point cloud input $X \in \mathbb{R}^{M \times 3}$, they construct an equivariant feature descriptor field $f(x|X)$ such that

$$f(x|X) = f(Tx|TX) \quad \forall T \in SE(3) \quad (3)$$

The descriptor field $f(x|X)$ is trained with self-supervised learning to encode the geometry of the target object. For the LfD step, they define the following energy function on the $SE(3)$ manifold

$$E(T) = \sum_{x \in \mathcal{X}_q} \left\| f(Tx|X) - f(\hat{T}x|\hat{X}) \right\|_1 \quad (4)$$

where $\mathcal{X}_q = \{x_1, x_2, \dots, x_{N_q}\} \in \mathbb{R}^{N_q \times 3}$ is a set of query points. \hat{T} and \hat{X} are the demonstration's grasp pose and the point cloud input, respectively. If multiple demonstrations are given, $f(\hat{T}x|\hat{X})$ are simply averaged over the demonstrations.

NDFs can learn simple pick-and-place tasks with only a few demonstrations ($5 \sim 10$). Moreover, the trained model shows impressive generalization capabilities for the target objects of unseen poses and unseen instances. However, the major limitation is that NDFs are not an end-to-end model. First, NDFs assume the point cloud input to be segmented from the background. In addition, NDFs assume large datasets of objects in the target object categories for the self-supervised learning phase. These are not trivial assumptions in practice.

B. Representation Theory of Lie Group

A representation D of a group G is a map from G to the space of linear operators acting on some vector space \mathcal{V} that has the following property for all $g, h \in G$,

$$D(g)D(h) = D(g \circ h) \quad (5)$$

Given vector spaces \mathcal{V} and \mathcal{W} and a function $f : \mathcal{V} \rightarrow \mathcal{W}$, f is said to be *equivariant* to a group G if

$$D_{\mathcal{W}}(g)f(v) = f(D_{\mathcal{V}}(g)v) \quad \forall g \in G, v \in \mathcal{V} \quad (6)$$

where $D_{\mathcal{V}}$ and $D_{\mathcal{W}}$ are some representations of G that linearly acts on \mathcal{V} and \mathcal{W} respectively.

Two different representations D and D' are said to be of *equivalence*² if there exists some non-degenerate change of basis S such that

$$D'(g) = SD(g)S^{-1} \quad \forall g \in G \quad (7)$$

A representation is said to be *reducible* if there exists some change of basis such that the representation can be decomposed (block-diagonalized) into smaller subspaces. An *irreducible representation* is a representation that cannot be reduced anymore.

For the $SO(3)$ group, any representation $D(R)$ for $R \in SO(3)$ can be reduced into a direct sum of $(2l+1) \times (2l+1)$ dimensional irreducible representations $D_l(R)$ of *degree* $l \in \{0, 1, 2, \dots\}$ such that

$$D(R) = S \left[\bigoplus_{n=1}^N D_{l_n}(R) \right] S^{-1} \quad \forall R \in SO(3) \quad (8)$$

where \bigoplus denotes a direct sum³. Although there are infinitely many equivalent representations for D_l , a particularly preferred choice is the *real basis*⁴. In this basis, all the representations D_l are orthogonal matrices. These matrices are called the (*real*) *Wigner D-matrices*. Details and the formulas can be found in [17].

$l \in \{0, 1, 2, \dots\}$ is called the *degree* of the representation. The $(2l+1)$ dimensional vectors that are transformed by $D_l(R)$ are called *type- l* vectors. Type- l vectors are identical to themselves when they are rotated by $\theta = 2\pi/l$. Type-0 vectors, or *scalars* are invariant to rotations. Type-1 vectors are the familiar 3-dimensional space vectors.

C. Equivariant Graph Neural Networks

Graph neural networks are often used to model point cloud data [18], [19], [20]. $SE(3)$ -equivariant graph neural networks [11], [12], [21] were proposed to exploit the rotation symmetry of graphs with spatial structures. In this work, we use *tensor field networks* (TFNs) [11] and the *$SE(3)$ -transformers* [12] as the backbone networks for our equivariant models. More detailed descriptions of these networks are provided in Appendix.

²Not to be confused with *equivariance*.

³Direct sum can be intuitively understood as a concatenation for vectors and a block-concatenation for matrices.

⁴Another commonly used choice of basis is the *spherical basis* where the representations are unitary and spherical harmonics are complex.

D. Equivariant Energy-Based Models

Equivariant EBMs on spaces where the symmetry group acts on (e.g., Euclidean space or N-body systems) have been investigated by [22], [13], [23]. However, no work has yet addressed an equivariant EBM on the group manifold itself. In this paper, we propose equivariant EBMs on the $SE(3)$ manifold.

III. METHODS

In this section, we present EDFs and the corresponding $SE(3)$ -equivariant energy-based models (EBM). EDFs are the equivariant extensions to NDFs [8] which are *invariant* descriptors in the context of the representation theory of the Lie group. We also reformulate the energy optimization problem of [8] into the equivariant distribution learning problem for the end-to-end learning. We illustrate our method in Fig. 2

A. Equivariant Descriptor Field

Consider a colored point cloud input with M points given by $X = \{(x_1, f_1), \dots, (x_M, f_M)\} \in \mathbb{R}^{M \times 6}$ where $x_i \in \mathbb{R}^3$ is the position and $f_i \in \mathbb{R}^3$ is the color vector of the i -th point. Note that M may vary between different point cloud inputs. Since color vectors are direct sums of three type-0 scalar features (red, green, and blue), they are invariant under rigid body transformations. Therefore, X transforms by a rigid body transformation $T = (R, t) \in SE(3)$ as

$$TX = \{(Rx_1 + t, f_1), \dots, (Rx_M + t, f_M)\} \quad (9)$$

We now define the EDF $f(x|X)$ as the direct sum of irreducible $SE(3)$ -equivariant vector fields whose n -th feature vector is a type- l_n vector, which is $(2l_n + 1)$ dimensional:

$$f(x|X) = \bigoplus_{n=1}^N f^{(n)}(x|X) \quad (10)$$

By a rigid body transformation $T \in SE(3)$, the EDF transforms equivariantly as follows:

$$f(Tx|TX) = D(R)f(x|X) \quad \forall T \in SE(3) \quad (11)$$

where $D(R) = \bigoplus_{n=1}^N D_{l_n}(R)$ is the direct sum of the Wigner D-Matrices of degree l_n in the real basis. Note that $D(R)$ is the orthogonal representation of the $SO(3)$ group such that

$$D(R)^T = D(R)^{-1} = D(R^{-1}) = D(R^T) \quad (12)$$

B. Equivariant Energy Function on $SE(3)$ Group

In this section, we propose a $SE(3)$ -equivariant energy function⁵

$$E_{\theta}(T|X) = \int d^3x \rho_{\theta}(x) \|f_{\theta}(Tx|X) - D(R)f_{Q;\theta}(x)\|^2 \quad (13)$$

where $\rho_{\theta}(x)$ is a learnable *query density* and $f_{Q;\theta}(x)$ is a learnable *query feature field*.

⁵Other variants of the energy function can be found in Appendix.

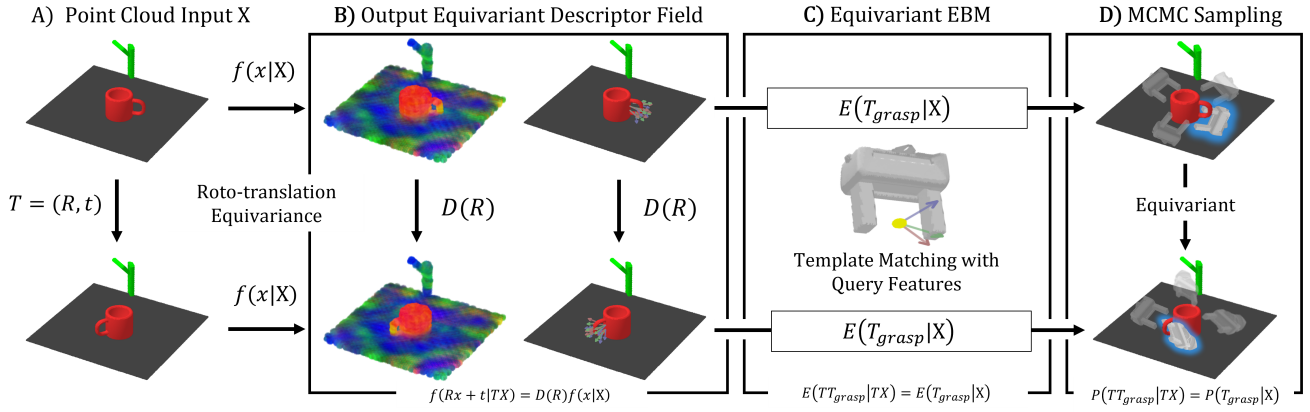


Fig. 2. The architecture for the picking model is illustrated in the figure. The placing model can be implemented similarly. A) The input to the model is given as the colored point cloud of a scene with a mug (red) and a hanger (green). The mug may transform by a rigid body transformation $T = (R, t) \in SE(3)$. Note that the illustrated transformation is *local*, in that only the mug transforms, and the background stays the same. B) The point cloud input is passed into the EDF model. We illustrate three type-0 scalar fields (left) and three type-1 vector fields (right) as the model’s outputs. The three fields are visualized as red, green, and blue, respectively. For clarity, only the vector fields near the handle are visualized. Note the equivariance of the output fields by the *local* $SE(3)$ transformation of the mug. Type-0 scalar fields are *invariant* such that the color remains the same after the transformation. In contrast, type-1 vector fields change their direction equivariantly according to the transformation. C) The feature fields are passed into the equivariant energy function. The energy function can be understood as a type-0 scalar field on the $SE(3)$ -manifold. D) The equivariant probability distribution can be constructed from the equivariant energy function. The end-effector poses can be sampled from the distribution by the MCMC algorithms in Section IV.

We define the corresponding energy-based model as follows:

$$P_{\theta}(T|X) = \frac{\exp[-E_{\theta}(T|X)]}{\int dT \exp[-E_{\theta}(T|X)]} \quad (14)$$

where dT is the invariant Haar measure such that the integral over $SE(3)$ group is invariant: $\int d(T'T) = \int dT$.

Now, we define the equivariance property of probability densities and functions on the $SE(3)$ manifold. We then show that the energy-based models with equivariant energy functions are also equivariant.

Definition 1: A X -conditioned scalar function $h(T|X) : SE(3) \times \mathbb{R}^{M \times 6} \rightarrow \mathbb{R}$ is $SE(3)$ -equivariant if

$$h(T|X) = h(T'T|T'X) \quad \forall T' \in SE(3)$$

Since we are dealing with an invariant measure, the equivariance for probability densities can be defined in a similar manner: A probability density $P(T|X)$ is $SE(3)$ -equivariant if $P(T|X) = P(T'T|T'X) \quad \forall T' \in SE(3)$.

Lemma 1: Consider an energy-based model conditioned by X as follows:

$$P(T|X) = \frac{\exp[-E(T|X)]}{\int dT \exp[-E(T|X)]} \quad (15)$$

(15) is then equivariant if the energy function $E(T|X)$ is equivariant, that is $E(T|X) = E(T'T|T'X) \quad \forall T' \in SE(3)$.

Proof:

$$\begin{aligned} P(T'T|T'X) &= \frac{\exp[-E(T'T|T'X)]}{\int dT \exp[-E(T|T'X)]} \\ &= \frac{\exp[-E(T'T|T'X)]}{\int dT \exp[-E(T'T|T'X)]} \\ &= \frac{\exp[-E(T|X)]}{\int dT \exp[-E(T|X)]} \\ &= P(T|X) \end{aligned}$$

Note that the group shift invariance of the integral is used in the second line, and the equivariance property of the energy function is used in the third line. ■

Now, we show that our energy function (13) is indeed $SE(3)$ -equivariant.

Theorem 1: The following energy function is $SE(3)$ -equivariant:

$$E_{\theta}(T|X) = \int d^3x \rho_{\theta}(x) \|f_{\theta}(Tx|X) - D(R)f_{Q;\theta}(x)\|^2$$

Proof:

$$\begin{aligned} E(T'T|T'X) &= \int d^3x \rho_{\theta}(x) \|f_{\theta}(T'Tx|T'X) - D(R')D(R)f_{Q;\theta}(x)\|^2 \\ &= \int d^3x \rho_{\theta}(x) \|D(R')f_{\theta}(Tx|X) - D(R')D(R)f_{Q;\theta}(x)\|^2 \\ &= \int d^3x \rho_{\theta}(x) \|f_{\theta}(Tx|X) - D(R)f_{Q;\theta}(x)\|^2 \\ &= E(T|X) \end{aligned}$$

Note that (11) is used in the third line, and $D(R)^T D(R) = I$ is used in the fourth line. ■

C. Implementation

Our method consists of two parts: The *picking model* and the *placing model*. The picking model consists of a single EDF model and the corresponding energy model. The placing model is similar to the picking model but has an additional EDF model which replaces the original query feature field. Therefore, the query feature field for the place model is $f_{Q;\theta}(x|X_{grasp})$ where X_{grasp} is the point cloud of the gripper with the grasped object. This architecture is analogous to the transport part of Transporter Networks [15]

where the query feature kernels that encode how the objects are grasped are template-matched (convolved) to the key feature field.

In practice, we use a weighted sum of the Dirac delta functions δ centered at query points as the query density.

$$\rho_\theta(x) = \sum_{i=1}^{N_q} w_i \delta(x - x_i) \quad (16)$$

where the query weight w_i and the position of the query point x_i are either predefined or learnable parameters. In this case, the integral of (13) is replaced to a much more tractable summation form as follows:

$$E_\theta(T|X) = \sum_{i=1}^N w_i \|f_\theta(Tx_i|X) - D(R)f_{Q_i}\|^2 \quad (17)$$

where $f_{Q_i} = f_{Q;\theta}(x_i)$ and $w_i = \rho_\theta(x_i)$.

Note that the L_2 energy version of (4) can be understood as a special case for (17), where $w_i = 1/N_q$ and all the field features are the *invariant* type-0 scalar fields.

For the backbone architectures to the EDF $f_\theta(x|X)$ we used SE(3)-Transformers [12]. However, self-attention cannot be applied to the last layer because the input points are different from the output transformed query points $\{Tx_i\}_{i=1}^{N_q}$. Therefore, we used TFNs [11] instead of SE(3) Transformers for the last layer of EDFs. We used the E3NN [24] package to implement the equivariant layers. We implemented equivariant layer normalizations for the stability of the learning.

For the computational efficiency and the locality of the algorithm, we impose the field values to be zero for the places farther than the field cutoff distance, which can be set as a hyperparameter. We set infinite energy for configurations outside the task space, thereby guaranteeing all the samples to be in the task space. Although not necessary, we also set high energies for configurations with no neighbor points within the field cutoff distance for faster sampling (See Sec. IV for the sampling). Details for the implementations can be found in the code.

IV. SAMPLING AND TRAINING

Direct sampling from the probability distribution in (14) cannot be done easily. Moreover, the integral in the denominator of (14) is intractable for the energy function of (17). Therefore, simple maximum likelihood learning cannot be used to train our models. In this section, we demonstrate the sampling strategy for our models using Markov Chain Monte-Carlo (MCMC). We also demonstrate the contrastive divergence based method for training our models.

A. Sampling

For the sampling, we combined the Metropolis-Hastings (MH) [25] algorithm and the Metropolis-adjusted Langevin algorithm (MALA) [26]. The MH algorithm is a propose-and-reject algorithm, where a proposal point x_p is sampled from the proposal distribution $Q(x_p|x_t)$. The proposed point x_p is stochastically accepted or rejected by the acceptance ratio $A = \min \left[1, \frac{P(x_p)Q(x_t|x_p)}{P(x_t)Q(x_p|x_t)} \right]$. If the proposal is accepted,

the next point is the proposed point, that is $x_{t+1} = x_p$. If rejected, the point remains the same, that is $x_{t+1} = x_t$. It is known that $P_t(x_t)$ converges to $P(x)$ as $t \rightarrow \infty$ for an arbitrary proposal distribution $Q(x_p|x_t)$. MALA is a special case of the MH algorithm where the new points are proposed with the Langevin dynamics.

It is known that typically MALA converges with much fewer iterations than MH when the variances of the proposal distributions are similar. However, MALA requires the gradient of the log probability, which is computationally expensive to calculate. In addition, to maintain the precision of the Langevin dynamics, the timestep of MALA cannot be arbitrarily high. Therefore, MALA is inappropriate for rapid initial exploration in broad workspaces. On the other hand, arbitrarily high variance can be used for the MH proposal. However, the MH algorithm suffers from a high rejection ratio near the minima. Therefore, we use the MH algorithm in the beginning for faster exploration. Once the sample points are settled near the minima, MALA is used to finetune the samples.

In the following paragraphs, we demonstrate the choice of the proposal distributions on the $SE(3)$ manifold. Note that the acceptance ratio A is a coordinate independent quantity. However, special care should be taken for the sampling to be coordinate independent when dealing with non-Euclidean manifolds such as the $SE(3)$ manifold.

1) *Proposal Distribution for MH*: The MH algorithm requires a proposal distribution. We decomposed the proposal step into 1) orientation proposal and 2) position proposal and used an isotropic Gaussian for the position proposal. For the orientation proposal, naive Gaussian sampling in axis-angle parametrization cannot be used when the variance is large. For a large variance, the tails of the Gaussian start to fold over, resulting in wrong estimates. Instead, we used $\mathcal{TG}_{SO(3)}$ which is the normal distribution on $SO(3)$ [27], [28], [29]. In the axis-angle parametrization, the axis is proposed uniformly from a unit sphere. The proposal distribution for the angle ω is as follows:

$$f_\epsilon(\omega) = \left[\sum_{l=0}^{\infty} (2l+1) e^{-\epsilon l(l+1)} \frac{\sin((2l+1)\omega/2)}{\sin \omega/2} \right] \quad (18)$$

For the sampling of ω , the Haar measure $(1 - \cos \omega)/\pi$ should be multiplied to $f_\epsilon(\omega)$. We used the inverse CDF sampling from $(1 - \cos \omega)/\pi \times f_\epsilon(\omega)$ as [29].

2) *Proposal Distribution for MALA*: Let \mathcal{V}_i be the i -th basis of the Lie algebra of an unimodular Lie group G . Consider the following stochastic process $g(t) \in G$ generated by a Lie algebra $\delta X(t) = \sum_i \delta X_i(t) \mathcal{V}_i \in T_e G$ such that

$$g(t) = g(0) \exp[\delta X(0)] \exp[\delta X(dt)] \cdots \exp[\delta X(t-dt)] \quad (19)$$

The Langevin dynamics for a Lie group is given as $\delta X_i(t) = -\mathcal{L}_{\mathcal{V}_i}[E(g)] dt + \sqrt{2} dW_i$ where $dW_i \sim \mathcal{N}(\mu = 0, \sigma = \sqrt{dt})$ is the white noise of the standard Wiener process and $\mathcal{L}_{\mathcal{V}} f = \left(\frac{d}{ds} f(g \exp[s\mathcal{V}]) \right) \Big|_{s=0}$ is the Lie derivative along \mathcal{V} . It is known that this process converges to $P_\infty(g) \propto \exp[-E(g)]$ when $t \rightarrow \infty$ [30].

Therefore, for the sampling procedure, one may sample δX_i from the $\mathcal{N}(\mu_i, \sigma)$ where $\mu_i = -\mathcal{L}_{\mathcal{V}_i}[E(g)]dt$ and $\sigma = \sqrt{2dt}$. The sampled δX_i is then exponentiated and applied to $g(t)$ as (19). However, dt should be very small to maintain the accuracy of the dynamics. For larger timesteps, naive Gaussian sampling tends to underestimate the variance of the diffusion for the $SO(3)$ part. Therefore, we approximate the SDE by sampling the noise from $\mathcal{IG}_{SO(3)}$ instead of Gaussian. Note that $\mathcal{IG}_{SO(3)}$ is a solution to the diffusion process on $SO(3)$ [27]. Therefore, when the Lie derivatives are sufficiently small, the approximation becomes accurate. In practice, we sample the noise R_ϵ from $\mathcal{IG}_{SO(3)}(\epsilon = \frac{\sigma^2}{2})$, take a matrix logarithm, then add to μ_i such that $\delta X(t)_i = \mu_i + [\log R_\epsilon]_i$ for the $SO(3)$ proposal. Instead of (18), we use the following formula which has better convergence property for small ϵ [27], [29]:

$$f_\epsilon(\omega) = (\sqrt{\pi}/2 \sin(\omega/2)) e^{(\epsilon - \omega^2/\epsilon)/4} \epsilon^{-3/2} \times \left\{ \omega + \sum_{n=1}^{\infty} (-1)^n e^{-\pi^2 n^2/\epsilon} \times \left[(\omega - 2\pi n) e^{n\pi\omega/\epsilon} + (\omega + 2\pi n) e^{-n\pi\omega/\epsilon} \right] \right\} \quad (20)$$

Note that for very small ϵ , $f_\epsilon(\omega) \propto e^{-\omega^2/4\epsilon} = e^{-\omega^2/2\sigma^2}$ which is Gaussian.

B. Training

We use the contrastive divergence (CD) [31], [32] algorithm for training our energy-based models. For the energy-based model (14), the gradient of the log-likelihood can be approximated with the CD gradient

$$\nabla_\theta \log P_\theta(x|X) \approx -\mathbb{E}_{P_0(x|X)} [\nabla_\theta E_\theta(x|X)] + \mathbb{E}_{P_n(x|X)} [\nabla_\theta E_\theta(x|X)] \quad (21)$$

where $P_0(x|X)$ is the target distribution and $P_n(x|X)$ is the n -step sample distribution of the MCMC that starts from $P_0(x|X)$.

V. EXPERIMENT AND RESULT

We evaluate the generalization capability of our models with three criteria: 1) Out-of-distribution (OoD) pose generalization, 2) Unseen instance generalization, and 3) Robustness to unseen visual distractors. We evaluate with a pick-and-place task similar to [8], where a mug should be picked and hung on the hanger’s hook. Ten demonstrations are provided to train the models. Note that all the demonstrations are given with a single identical mug with upright poses only.

For the test environment, we use PyBullet [33] simulator for the experiments. We use the Franka Panda manipulator with a custom end-effector. We use IKFast [34] with Pybullet-Planning [35] for the inverse kinematics. Three simulated depth cameras are used to observe the point clouds. Since motion planning is not in the scope of our work, we assume no collision between the environment and the robot links except for the hand link. We also allow the robot to teleport to reach pre-grasp and pre-place poses in

TABLE I
UNSEEN POSE SUCCESS RATE

	Pick	Place	Pick-and-Place
Upright poses	0.95 (95/100)	0.96 (92/95)	0.92 (92/100)
Lying (OoD) poses	0.94 (94/100)	0.95 (90/94)	0.90 (90/100)

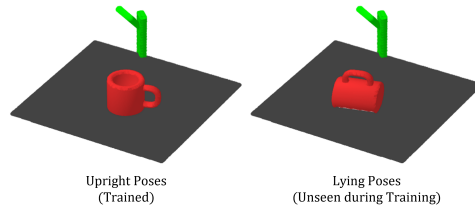


Fig. 3. We evaluate the models’ generalization capability to unseen OoD poses of the target objects with two distinct poses: Upright poses (Left) and Lying poses (Right). Only upright poses were given during the training. Lying poses were never given during the training steps. The planar configurations (x , y , and θ) of the mug and the hanger are randomized among different seeds.

order to eliminate the unnecessary influence of the motion planners. However, we fully simulate the trajectories of all the task-relevant primitives (e.g., grasping, releasing, lifting). Since the base of the manipulator is fixed, some end-effector orientations cannot be reached. In this case, we allow the robot to consider the opposite orientation along the end-effector axis.

We empirically find that the MCMC algorithm converges after running the MH algorithm for around 3000 steps and the MALA for around 500 steps. However, waiting for the algorithm to fully converge takes an impractical amount of time (more than a minute). Therefore, we prematurely terminate the MCMC algorithm and take the minimum energy sample instead. We find that this strategy yields reasonable performance. Specifically, we run the MH algorithm for 500 steps and then run the MALA for 100 steps for the sampling. We parallelize the sampling with 100 different seeds. We then take the pose with the lowest energy from the last 50 steps.

All the experiments were done with CPUs for reproducibility. On average, the wall-clock inference times are 19 seconds for the pick tasks and 13 seconds for the place tasks on an Intel i7-10875H CPU. We also test with an Nvidia RTX 3090 GPU, but it turns out to be slower than the CPU. We presume this is due to the non-parallel nature of the MCMC algorithms.

A. Unseen Pose Generalization

We evaluate the generalization capability of the trained models with previously unseen OoD poses of the target object (See Fig. 3). We examine the performance with 100 samples with the same mug used for training but with lying poses, which were never given during the training phase. We find no significant difference in the performance between different poses. The results are summarized in Table I.

TABLE II
UNSEEN INSTANCE SUCCESS RATE

	Pick	Place	Pick-and-Place
Mug 1	0.92 (23/25)	0.78 (18/23)	0.72 (18/25)
Mug 2	0.100 (25/25)	0.92 (23/25)	0.92 (23/25)
Mug 3	0.88 (22/25)	0.77 (17/22)	0.68 (17/25)
Mug 4	0.80 (20/25)	0.70 (14/20)	0.56 (14/25)
Avg.	0.90 (90/100)	0.80 (72/90)	0.72 (72/100)

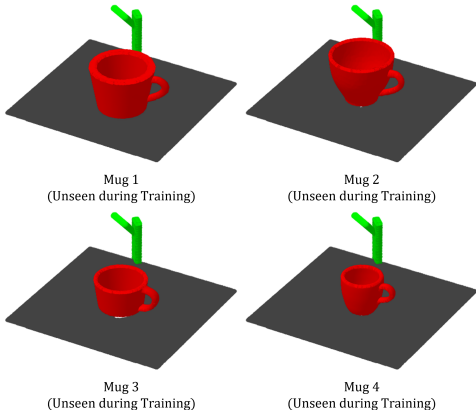


Fig. 4. We evaluate the models’ generalization capability to unseen target object instances in the same category. We test with four different instances of the mug that were never given during the training steps. The planar configurations (x , y , and θ) of the mugs and the hanger are randomized among different seeds.

B. Unseen Instance Generalization

We evaluate the generalization capability of the trained models with previously unseen target object instances in the same category (See Fig 4). We examine the performance with four different mug/cup instances that were never given during the training phase. We examine 100 samples for each mug/cup instance. The results are summarized in Table II.

C. Unseen Visual Distractor Generalization

We evaluate the generalization capability of the trained models in the presence of previously unseen visual distractors (See Fig. 5). Since our models do not rely on any segmentation algorithms, robustness in the presence of previously unseen distractors is an important property. The results are summarized in Table III.

VI. DISCUSSION AND CONCLUSION

In this work, we presented fully end-to-end $SE(3)$ -equivariant models for visual robotic manipulation learning. We formulated novel $SE(3)$ -equivariant descriptor fields and energy-based models based on the representation theory of the Lie group that allow highly sample efficient and generalizable learning. We also provided working strategies for sampling from our energy-based models on the $SE(3)$ manifold. The models can learn visual pick-and-place tasks with only ~ 10 demonstrations in a fully end-to-end manner. Moreover, we showed that the trained models could generalize to the tasks with unseen target object poses, unseen target object instances, and unseen visual distractors.

TABLE III
UNSEEN VISUAL DISTRACTOR SUCCESS RATE

	Pick	Place	Pick-and-Place
Distractors	0.68 (68/100)	0.85 (58/68)	0.58 (58/100)

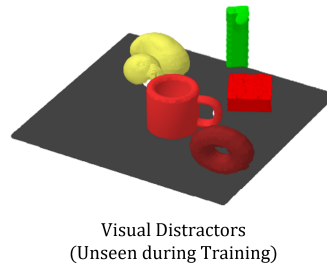


Fig. 5. We evaluate the models’ generalization capability in the presence of unseen visual distractors. The visual distractors were never given during the training steps. The planar configurations (x , y , and θ) of the mug, the distractors, and the hanger are randomized among different seeds.

However, our method has several limitations that should be addressed in future works. The most severe limitation is the long inference time due to the MCMC sampling. Faster and more efficient generative models should be developed for real-time inference.

Another limitation is the strict $SE(3)$ -equivariance assertion of the models. Global $SE(3)$ symmetry cannot be strictly kept in most visual manipulation problems due to the gravity, occlusions, deformations of objects, and the background scenes. Therefore, we took special care in the design to make the models capture only the local $SE(3)$ symmetries. Nevertheless, our models may perform significantly worse than non-equivariant models when the local $SE(3)$ symmetries are severely broken. Hence, models with relaxed forms of the $SE(3)$ -equivariance would be required to guarantee the minimum performance for the tasks without the $SE(3)$ symmetry while enjoying the equivariance for tasks with the $SE(3)$ symmetry.

Although we only demonstrated our models with robotic manipulation tasks, our models can be generally applied to any $SE(3)$ -symmetric problems with a point cloud as the input and a $SE(3)$ transformation as the output. Therefore, we expect our novel equivariant energy-based models to be useful in various domains such as protein folding and pose estimation problems, especially when the samples are rare.

APPENDIX

A. Equivariant Graph Neural Networks

1) *Tensor Product and Spherical Harmonics*: Given two vectors u and v of type- l_1 and $-l_2$, the tensor product $u \otimes v$ transforms by a rotation $R \in SO(3)$ as

$$u \otimes v \rightarrow (D_{l_1}(R)u) \otimes (D_{l_2}(R)v) \quad (22)$$

Tensor products are important because they can be used to construct new vectors of different types. By a change of basis the tensor product $u \otimes v$ can be decomposed into a direct

sum of type- l vectors using the *Clebsch-Gordan coefficients* [11], [36], [37] as follows:

$$(u \otimes v)_m^{(l)} = \sum_{m_1=-l_1}^{l_1} \sum_{m_2=-l_2}^{l_2} C_{(l_1, m_1)(l_2, m_2)}^{(l, m)} u_{m_1}^{(l_1)} v_{m_2}^{(l_2)} \quad (23)$$

where the Clebsch-Gordan coefficients $C_{(l_1, m_1)(l_2, m_2)}^{(l, m)}$ are nonzero for $|l_1 - l_2| \leq l \leq l_1 + l_2$ only.

The (real) spherical harmonics $Y_m^{(l)}(x/\|x\|)$ are orthonormal functions that form the complete basis of the Hilbert space on a sphere. $l \in \{0, 1, 2, \dots\}$ is called the *degree* and $m \in \{-l, \dots, l\}$ is called the *order* of the spherical harmonic function.

Consider the following $(2l + 1)$ -dimensional vector field $Y^{(l)} = (Y_{m=-l}^l, \dots, Y_{m=l}^l)$. By a 3-dimensional rotation $R \in SO(3)$, $Y^{(l)}$ transforms like a type- l vector field such that

$$Y^{(l)}(R(x/\|x\|)) = D_l(R)Y^{(l)}(x/\|x\|) \quad (24)$$

2) *Tensor Field Networks*: Tensor field networks (TFNs) [11] are $SE(3)$ -equivariant models for generating representation-theoretic vector fields from a point cloud input. TFNs construct equivariant output feature vectors from equivariant input feature vectors and spherical harmonics. Spatial convolutions and tensor products are used for the equivariance.

Consider a featured point cloud input with M points given by $X = \{(x_1, f_1), \dots, (x_M, f_M)\}$ where $x_i \in \mathbb{R}^3$ is the position and f_i is the equivariant feature vector of the i -th point. Let f_i be decomposed into N vectors such that $f_i = \bigoplus_{n=1}^N f_i^{(n)}$, where $f_i^{(n)}$ is a type- l_n vector, which is $(2l_n + 1)$ dimensional. Then the input feature field $f_{(in)}(x|X)$ generated by the point cloud input X can be defined as

$$f_{(in)}(x|X) = \sum_{j=1}^M f_{(in),j} \delta(x - x_j) \quad (25)$$

where $\delta(x - x_j)$ is the Dirac delta function centered at x_j . Note that $f_{(in)}$ is $SE(3)$ equivariant:

$$f_{(in)}(Tx|TX) = D(R)f_{(in)}(x|X) \quad \forall T = (R, t) \in SE(3)$$

where $R \in SO(3)$, $t \in \mathbb{R}^3$ and $D(R) = \bigoplus_{n=1}^N D_{l_n}(R)$. Note that T acts on x and X such that $Tx = Rx + t$ and $TX = \{(Rx_1 + t, D(R)f_1), \dots, (Rx_M + t, D(R)f_M)\}$.

Now consider the following output feature field of a convolution layer

$$f_{(out)}(x|X) = \bigoplus_{n'=1}^{N'} f_{(out)}^{(n')}(x|X)$$

with the kernel $W(x - y) \in \mathbb{R}^{\dim(f_{(out)}) \times \dim(f_{(in)})}$ whose (n', n) -th block $W^{n'n}(x - y) \in \mathbb{R}^{(2l_{n'}+1) \times (2l_n+1)}$ is

$$\begin{aligned} [W^{n'n}(x)]_{m'm} &= \sum_{J=|l_{n'}-l_n|}^{l_{n'}+l_n} \phi_J^{n'n}(\|x\|) \\ &\times \sum_{k=-J}^J C_{(J,k)(l_n, m)}^{(l_{n'}, m')} Y_k^{(J)}(x/\|x\|) \end{aligned} \quad (26)$$

Here, $\phi_J^{n'n}(\|x\|)$ is a learnable radial function, $Y_k^{(J)}$ is the k -th component of the real spherical harmonics of degree k , and C is the Clebsch-Gordan coefficients in the real basis. The output $f_{(out)}(x)$ of the following convolution

$$\begin{aligned} f_{(out)}(x|X) &= \int d^3y W(x - y) f_{(in)}(y|X) \\ &= \sum_j W(x - x_j) f_{(in),j} \end{aligned} \quad (27)$$

is proven to be equivariant [11], [12]. Note that the output equivariant feature vectors are constructed by the tensor product of input equivariant feature vectors and the spherical harmonics, which encode the spatial information.

3) *SE(3)-Transformers*: The $SE(3)$ -Transformers [12] are variants of TFNs with self-attention. Consider the case that the output field is also of the form

$$f_{(out)}(x|X) = \sum_{j=1}^M f_{(out),j} \delta(x - x_j) \quad (28)$$

where x_i is the same point as that of the point cloud input X . The $SE(3)$ -Transformers apply type-0 (scalar) self-attention α_{ij} to (27):

$$\begin{aligned} f_{(out),i} &= \bigoplus_{n'} \sum_{n=1}^N W_{(S)}^{n'n} f_{(in),j}^{(n)} \\ &+ \sum_{j \neq i} \alpha_{ij} W(x - x_j) f_{(in),j} \end{aligned} \quad (29)$$

where the $W_{(S)}^{n'n}$ term is called the *self-interaction* [11]. $W_{(S)}^{n'n}$ is nonzero only when $l'_n = l_n$. The self-interaction occurs where $i = j$ such that $W(x_i - x_j) = W(0)$. The self-interaction term is needed because W is a linear combination of the spherical harmonics which are not well defined in $x = 0$.

B. Variants of the $SE(3)$ -Equivariant Energy Function

In the previous sections, we only introduced the equivariant energy function with a square error form (13). Although we find that (13) is reasonably good for our tasks, the square error term may be too strict in some tasks. Thus, the corresponding energy-based models can be fragile to outliers. Therefore, we propose two variants of (13), the inner-product variant and the L_1 -norm variant.

1) *Inner Product Form*: The following energy function is equivariant

$$E_\theta(T|X) = \int d^3x \rho_\theta(x) \langle f_\theta(Tx|X), D(R)f_{Q;\theta}(x) \rangle \quad (30)$$

where $\langle \cdot, \cdot \rangle$ denotes the inner product. The proof for the equivariance is straightforward using the orthogonality of the real Wigner D-matrix $D(R)$. One may also consider using a normalized cosine distance instead of the inner product.

2) L_1 Form: The L_1 -norm is often preferred over the L_2 -norm for their robustness. However, unlike the L_2 -norm, the L_1 -norm is not equivariant by itself. Therefore, we propose the *irrep-wise L_1 -norm*. For an equivariant vector $f = \bigoplus_{n=1}^N f^{(n)}$, the equivariant irrep-wise L_1 -norm can be defined as

$$\|f\|_1^{(T)} = \sum_{n=1}^N \|f^{(n)}\| \quad (31)$$

Now, consider an EDF $f_\theta(x|X)$ and a query feature field $f_{Q;\theta}(x)$. The following energy function is then equivariant.

$$E_\theta(T|X) = \int d^3x \rho_\theta(x) \|f_\theta(Tx|X) - D(R)f_{Q;\theta}(x)\|_1^{(T)} \quad (32)$$

REFERENCES

- [1] D. Kalashnikov, A. Ipran, P. Pastor, J. Ibarz, A. Herzog, E. Jang, D. Quillen, E. Holly, M. Kalakrishnan, V. Vanhoucke, *et al.*, “Qt-opt: Scalable deep reinforcement learning for vision-based robotic manipulation (2018),” *arXiv preprint arXiv:1806.10293*, 2018.
- [2] S. Levine, C. Finn, T. Darrell, and P. Abbeel, “End-to-end training of deep visuomotor policies,” *The Journal of Machine Learning Research*, vol. 17, no. 1, pp. 1334–1373, 2016.
- [3] J.-H. Lee and J. Choi, “Attaining interpretability in reinforcement learning via hierarchical primitive composition,” *arXiv preprint arXiv:2110.01833*, 2021.
- [4] H. Ravichandar, A. S. Polydoros, S. Chernova, and A. Billard, “Recent advances in robot learning from demonstration,” *Annual Review of Control, Robotics, and Autonomous Systems*, vol. 3, pp. 297–330, 2020.
- [5] B. D. Argall, S. Chernova, M. Veloso, and B. Browning, “A survey of robot learning from demonstration,” *Robotics and autonomous systems*, vol. 57, no. 5, pp. 469–483, 2009.
- [6] A. Zeng, K.-T. Yu, S. Song, D. Suo, E. Walker, A. Rodriguez, and J. Xiao, “Multi-view self-supervised deep learning for 6d pose estimation in the amazon picking challenge,” in *2017 IEEE international conference on robotics and automation (ICRA)*. IEEE, 2017, pp. 1386–1383.
- [7] X. Deng, Y. Xiang, A. Mousavian, C. Eppner, T. Bretl, and D. Fox, “Self-supervised 6d object pose estimation for robot manipulation,” in *2020 IEEE International Conference on Robotics and Automation (ICRA)*. IEEE, 2020, pp. 3665–3671.
- [8] A. Simeonov, Y. Du, A. Tagliasacchi, J. B. Tenenbaum, A. Rodriguez, P. Agrawal, and V. Sitzmann, “Neural descriptor fields: SE(3)-equivariant object representations for manipulation,” *arXiv preprint arXiv:2112.05124*, 2021.
- [9] P. R. Florence, L. Manuelli, and R. Tedrake, “Dense object nets: Learning dense visual object descriptors by and for robotic manipulation,” *arXiv preprint arXiv:1806.08756*, 2018.
- [10] T. D. Kulkarni, A. Gupta, C. Ionescu, S. Borgeaud, M. Reynolds, A. Zisserman, and V. Mnih, “Unsupervised learning of object keypoints for perception and control,” *Advances in neural information processing systems*, vol. 32, 2019.
- [11] N. Thomas, T. Smidt, S. Kearnes, L. Yang, L. Li, K. Kohlhoff, and P. Riley, “Tensor field networks: Rotation-and translation-equivariant neural networks for 3d point clouds,” *arXiv preprint arXiv:1802.08219*, 2018.
- [12] F. Fuchs, D. Worrall, V. Fischer, and M. Welling, “SE(3)-transformers: 3d roto-translation equivariant attention networks,” *Advances in Neural Information Processing Systems*, vol. 33, pp. 1970–1981, 2020.
- [13] J. Wu, T. Shen, H. Lan, Y. Bian, and J. Huang, “SE(3)-equivariant energy-based models for end-to-end protein folding,” *bioRxiv*, 2021.
- [14] X. Li, Y. Weng, L. Yi, L. Guibas, A. L. Abbott, S. Song, and H. Wang, “Leveraging SE(3) equivariance for self-supervised category-level object pose estimation,” *arXiv preprint arXiv:2111.00190*, 2021.
- [15] A. Zeng, P. Florence, J. Tompson, S. Welker, J. Chien, M. Attarian, T. Armstrong, I. Krasin, D. Duong, V. Sindhwani, *et al.*, “Transporter networks: Rearranging the visual world for robotic manipulation,” *arXiv preprint arXiv:2010.14406*, 2020.
- [16] T. Cohen and M. Welling, “Group equivariant convolutional networks,” in *International conference on machine learning*. PMLR, 2016, pp. 2990–2999.
- [17] G. Aubert, “An alternative to wigner d-matrices for rotating real spherical harmonics,” *AIP Advances*, vol. 3, no. 6, p. 062121, 2013.
- [18] Y. Wang, Y. Sun, Z. Liu, S. E. Sarma, M. M. Bronstein, and J. M. Solomon, “Dynamic graph cnn for learning on point clouds,” *Acm Transactions On Graphics (tog)*, vol. 38, no. 5, pp. 1–12, 2019.
- [19] G. Te, W. Hu, A. Zheng, and Z. Guo, “Rgcnn: Regularized graph cnn for point cloud segmentation,” in *Proceedings of the 26th ACM international conference on Multimedia*, 2018, pp. 746–754.
- [20] W. Shi and R. Rajkumar, “Point-gnn: Graph neural network for 3d object detection in a point cloud,” in *Proceedings of the IEEE/CVF conference on computer vision and pattern recognition*, 2020, pp. 1711–1719.
- [21] C. Deng, O. Litany, Y. Duan, A. Poulencard, A. Tagliasacchi, and L. J. Guibas, “Vector neurons: A general framework for SO(3)-equivariant networks,” in *Proceedings of the IEEE/CVF International Conference on Computer Vision*, 2021, pp. 12 200–12 209.
- [22] P. Jaini, L. Holdijk, and M. Welling, “Learning equivariant energy based models with equivariant stein variational gradient descent,” in *Advances in Neural Information Processing Systems*, M. Ranzato, A. Beygelzimer, Y. Dauphin, P. Liang, and J. W. Vaughan, Eds., vol. 34. Curran Associates, Inc., 2021, pp. 16 727–16 737. [Online]. Available: <https://proceedings.neurips.cc/paper/2021/file/8b9e7ab295e87570551db122a04c6f7c-Paper.pdf>
- [23] J. J. Kivinen and C. K. Williams, “Transformation equivariant boltzmann machines,” in *International Conference on Artificial Neural Networks*. Springer, 2011, pp. 1–9.
- [24] M. Geiger, T. Smidt, A. M., B. K. Miller, W. Boomsma, B. Dice, K. Lapchevskyi, M. Weiler, M. Tyszkiewicz, S. Batzner, D. Madiseti, M. Uhrin, J. Frellsen, N. Jung, S. Sanborn, M. Wen, J. Rackers, M. Rød, and M. Bailey, “Euclidean neural networks: e3nn,” apr 2022. [Online]. Available: <https://doi.org/10.5281/zenodo.6459381>
- [25] W. K. Hastings, “Monte carlo sampling methods using markov chains and their applications,” 1970.
- [26] J. Besag, “Comments on “representations of knowledge in complex systems” by u. grenander and mi miller,” *J. Roy. Statist. Soc. Ser. B*, vol. 56, no. 591–592, p. 4, 1994.
- [27] D. I. Nikolayev and T. I. Savyolov, “Normal distribution on the rotation group SO(3),” *Textures and Microstructures*, vol. 29, 1970.
- [28] T. I. T. Savyolova, “Normal distributions on SO(3),” in *Programming And Mathematical Techniques In Physics-Proceedings Of The Conference On Programming And Mathematical Methods For Solving Physical Problems*. World Scientific, 1994, p. 220.
- [29] A. Leach, S. M. Schmon, M. T. Degiacomi, and C. G. Willcocks, “Denosing diffusion probabilistic models on SO(3) for rotational alignment,” in *ICLR 2022 Workshop on Geometrical and Topological Representation Learning*, 2022.
- [30] G. S. Chirikjian, *Stochastic models, information theory, and Lie groups, volume 2: Analytic methods and modern applications*. Springer Science & Business Media, 2011, vol. 2.
- [31] G. E. Hinton, “Training products of experts by minimizing contrastive divergence,” *Neural computation*, vol. 14, no. 8, pp. 1771–1800, 2002.
- [32] M. A. Carreira-Perpinan and G. Hinton, “On contrastive divergence learning,” in *International workshop on artificial intelligence and statistics*. PMLR, 2005, pp. 33–40.
- [33] E. Coumans and Y. Bai, “Pybullet, a python module for physics simulation for games, robotics and machine learning,” <http://pybullet.org>, 2016–2021.
- [34] R. Diankov, “Automated construction of robotic manipulation programs,” Ph.D. dissertation, Carnegie Mellon University, Robotics Institute, August 2010. [Online]. Available: http://www.programmingvision.com/rosen_diankov_thesis.pdf
- [35] C. R. Garrett, “Pybullet planning,” <https://pypi.org/project/pybullet-planning/>, 2018.
- [36] A. Zee, *Group theory in a nutshell for physicists*. Princeton University Press, 2016, vol. 17.
- [37] D. J. Griffiths and D. F. Schroeter, *Introduction to quantum mechanics*. Cambridge university press, 2018.